ADVANCED MATERIALS
www.advmat.de

Interlayer-Spacing-Regulated $VOPO_4$ Nanosheets with Fast Kinetics for High-Capacity and Durable Rechargeable Magnesium Batteries

Limin Zhou, Qi Liu, Zihe Zhang, Kai Zhang, Fangyu Xiong, Shuangshuang Tan, Qinyou An, Yong-Mook Kang, Zhen Zhou,* and Liqiang Mai**

Owing to the low-cost, safety, dendrite-free formation, and two-electron redox properties of magnesium (Mg), rechargeable Mg batteries are considered as promising next-generation secondary batteries with high specific capacity and energy density. However, the clumsy Mg^{2+} with high polarity inclines to sluggish Mg insertion/deinsertion, leading to inadequate reversible capacity and rate performance. Herein, 2D $VOPO_4$ nanosheets with expanded interlayer spacing (1.42 nm) are prepared and applied in rechargeable magnesium batteries for the first time. The interlayer expansion provides enough diffusion space for fast kinetics of $MgCl^+$ ion flux with low polarization. Benefiting from the structural configuration, the Mg battery exhibits a remarkable reversible capacity of 310 mAh g^{-1} at 50 mA g^{-1}, excellent rate capability, and good cycling stability (192 mAh g^{-1} at 100 mA g^{-1} even after 500 cycles). In addition, density functional theory (DFT) computations are conducted to understand the electrode behavior with decreased $MgCl^+$ migration energy barrier compared with Mg^{2+}. This approach, based on the regulation of interlayer distance to control cation insertion, represents a promising guideline for electrode material design on the development of advanced secondary multivalent-ion batteries.

Although lithium-ion batteries have been commercial since the early 1990s, the issues of resource sustainability and safety as well as inadequate energy density continue to draw much attention.[1–4] An alternative solution to address these problems for large-scale application is to explore promising candidate with cost priority and energy density requirement. Among the beyond Li-ion chemistry, magnesium metal anode as two-charge carrier, in particular, has a high theoretical volumetric capacities of 3833 mAh cm^{-3} (vs 2046 mAh cm^{-3} for Li) and dendrite-free property.[5–9] Also, Mg content is abundant in the earth curst, and they are intrinsically stable and much safer when exposed to air.[6,10] Despite these potential merits of magnesium over lithium as anode materials, the development of cathode materials for rechargeable magnesium batteries is curbed by high polarization arising from the interaction between Mg^{2+} and host materials.[11–13]

Benefitting from effective and simple ion insertion/deinsertion chemistry, 2D-layered materials have been widely studied for magnesium batteries.[14–17] For example, a layered TiS_2 provides a reversible Mg-storage capacity of 115 mAh g^{-1} at C/10 (12 mA g^{-1}) and 60 °C.[17] The cubic Ti_2S_4 prepared through oxidized extraction is capable of delivering a reversible capacity of 200 and 150 mAh g^{-1} on subsequent cycles at 60 °C.[16] Owing to diffusion dynamics limitation, both the layered host materials were, however, measured at elevated temperature. Meaningfully, Yao and co-workers altered inserted cation through the introduction of additive (1-butyl-1-methylpyrrolidinium chloride, PY14Cl) into electrolyte, achieving a reversible capacity of 173 mAh g^{-1} at 0.1 C (24 mA $g_{TiS_2}^{-1}$).[14] Inspired by the relationship between interlayer spacing and intercalation species, it is well worth attempting novel layered materials with adjustable interlayer distance, which simultaneously deliver high specific capacity, excellent rate capability, and cycling stability.

Compared with extensively reported layer dichalcogenides,[15,17] $VOPO_4$, as polyanion-type layered materials, is characteristic of corner-sharing VO_6 octahedra linking to PO_4 tetrahedra[18–20] and identified as an alternative architecture for energy storage. In addition, vacant coordination sites among

L. Zhou, Q. Liu, F. Xiong, S. Tan, Prof. Q. An, Prof. L. Mai
State Key Laboratory of Advanced Technology for Materials Synthesis and Processing
International School of Materials Science and Engineering
Wuhan University of Technology
Hubei, Wuhan 430070, China
E-mail: anqinyou86@whut.edu.cn; mlq518@whut.edu.cn
Z. Zhang, Prof. Z. Zhou
School of Materials Science and Engineering
Key Laboratory of Advanced Energy Materials Chemistry (Ministry of Education)
Institute of New Energy Material Chemistry
Collaborative Innovation Center of Chemical Science and Engineering (Tianjin)
National Institute for Advanced Materials
Nankai University
Tianjin 300071, China
E-mail: zhouzhen@nankai.edu.cn
Dr. K. Zhang, Prof. Y.-M. Kang
Department of Energy and Materials Engineering
Dongguk University-Seoul
Seoul 100-715, Republic of Korea
The ORCID identification number(s) for the author(s) of this article can be found under https://doi.org/10.1002/adma.201801984.

DOI: 10.1002/adma.201801984

restacking layers can afford cation intercalation due to the five-coordination circumstance of vanadium ion.[21] Spurred by the excellent electrochemical performance of $VOPO_4$ as cathode material for lithium-/sodium-ion batteries,[22–24] one wants to know if the robust structure with controlled interlayer spacing could be applied in multivalence batteries. To our best knowledge, there is no report about using $VOPO_4$ as a positive electrode for magnesium batteries.

Herein, we prepared $VOPO_4$ nanosheets with expanded layer spacing (from 0.74 to 1.42 nm) by a facile ultrasonicated exfoliation and self-assembly route. The expanded $VOPO_4$ architecture exhibits a reversible Mg-storage capacity of 310 mAh g^{-1}, high rate capability (275, 220, 175, 140, and 109 mAh g^{-1} at 100, 200, 500, 1000, and 2000 mA g^{-1}, respectively), and superior cycling stability (192 mAh g^{-1} at 100 mA g^{-1} even after 500 cycles). The outstanding electrochemical performance is associated with $MgCl^+$ intercalation, featuring half of Mg^{2+} polarization based on the increasing layer distance and further contributing to fast ion diffusion kinetics, which has been validated by X-ray photoelectron spectroscopy (XPS) and energy dispersive spectroscopy (EDS) analysis as well as computations.

The pure $VOPO_4 \cdot 2H_2O$ bulk was obtained by a hydrothermal method (Experimental Section, Supporting Information). Briefly, V_2O_5 powders and concentrated H_3PO_4 as raw materials were put into a 100 mL Teflon vessel and then heated at 120 °C for 16 h. The product was named as OH-$VOPO_4$. The expanded $VOPO_4$ nanosheets were synthesized by displacement reaction with phenylamine (PA) molecules (Figure S1a, Supporting Information), and the sample was labeled as PA-$VOPO_4$.

Figure 1a presents the X-ray diffraction (XRD) patterns of the as-prepared OH-$VOPO_4$ bulk and PA-$VOPO_4$ nanosheets. All peaks of the OH-$VOPO_4$ readily belong to space group *P*4/*nmm*, consistent with the position of tetragonal $VOPO_4 \cdot 2H_2O$ (JCPDS No. 84-0111). According to Bragg's equation ($2d\sin\theta = n\lambda$), the interlayer distance of OH-$VOPO_4$ is calculated to be 0.74 nm, identical to previous report.[20,23] Upon intercalation of PA molecules, the strong peak of (001) plane is substantially shifted toward lower angle (6.2°), implying the increasing of interlayer distance to 1.42 nm. Other peaks also weaken and vanish because of the decreasing of oxide crystallinity.[20] The content of H_2O and PA molecular can be calculated from the thermogravimetric analysis (TGA) of the OH-$VOPO_4$ and PA-$VOPO_4$ samples (Figure 1b). From which, we can see that the weight loss of the OH-$VOPO_4$ and PA-$VOPO_4$ is ≈18% and ≈30%, respectively, corresponding to $2H_2O$ per molecule in OH-$VOPO_4$ and 0.4PA in PA-$VOPO_4$. In addition, the analysis of CHN test presents 2.91 wt% of N elemental content, which approximately coincides with the TGA results. Figure S1b (Supporting Information) displays the Fourier transform infrared (FTIR) spectra of the two samples, consistent with $VOPO_4 \cdot 2H_2O$ and products treated in neat aniline.[25] The scanning electron microscopy (SEM) and transmission electron microscopy (TEM) images shown in Figure 1c,d demonstrate typical layered structure of the PA-$VOPO_4$ nanosheets with the plane size of 1 µm. Moreover, the expanded interlayer distance is observed by high-resolution TEM (HRTEM) image. As shown in Figure 1e, the PA-$VOPO_4$ nanosheets display well-defined layered architecture with ≈1.4 nm interlayer distance. This value enables layered structure to accommodate bilayer PA arrangement (inset of Figure 1e) since the maximum distance of PA molecule is roughly 0.57 nm.[20,25] The EDS elemental mapping of the PA-$VOPO_4$ nanosheets (Figure 1f) shows the evenly distribution of V, O, P, and N elements, further revealing the successful exchange with PA molecules. The morphology of OH-$VOPO_4$ bulk was demonstrated in Figure S2 (Supporting Information), which also possesses layered structure but tightly stacked and high crystalline character verified by the selected-area electron diffraction (SAED).

To examine the electrochemical behavior, the compatibility of Mg foil with all phenyl complex (APC) electrolyte in magnesium battery system was first evaluated (Figure S3, Supporting Information), in which the overpotential for Mg deposition is close to that of previous literature reported,[26] and the stripping/plating efficiency is ≈100%. **Figure 2**a demonstrates the charge/discharge profiles of the OH-$VOPO_4$ bulk and PA-$VOPO_4$ nanosheets at 100 mA g^{-1} and 50th cycle. It can be seen that OH-$VOPO_4$ possesses relatively large polarization and inferior specific capacity compared with PA-$VOPO_4$, illustrating that the expanded interlayer distance is convenient for cation shutting to improve diffusion kinetics. Considering the discrepancy of molar mass between OH-$VOPO_4$ and PA-$VOPO_4$, Mg-storage quantity of each mole molecular is given in Figure S4 (Supporting Information). The PA-$VOPO_4$ nanosheets enable the interlayer configuration to achieve 1.9 charge transfer. As seen in Figure 2b, both OH-$VOPO_4$ bulk and PA-$VOPO_4$ nanosheets are able to deliver above 300 mAh g^{-1} of Mg-storage capacity at 50 mA g^{-1}, attributing to the major capacity contribution stemming from diffusion controlled process.[23] And the volumetric specific capacity of PA-$VOPO_4$ is calculated to be 237.1 Ah L^{-1}, lower than 519 Ah L^{-1} of Mo_6S_8 because of the expanded interlayer distance. As current densities increase, the PA-$VOPO_4$ nanosheets render excellent reversible capacities of 275, 220, 175, 140, 109 mAh g^{-1} at 100, 200, 500, 1000, 2000 mA g^{-1}, respectively. The corresponding charge/discharge curves display that the polarization gradually increases and the voltage platform disappears with the increasing of current density (Figure S5, Supporting Information). Nevertheless, the capacity of OH-$VOPO_4$ bulk drastically attenuated with the increase of cycle number and current density. When the current density returns back to 200 mA g^{-1}, worst of all, the capacity is only 170 mAh g^{-1} and could not recover to preceding capacity. Figure 2c displays the charge/discharge curves of PA-$VOPO_4$ nanosheets at different cycles. Except for partial capacity decay with the prolonged cycle, the discharge plateau of PA-$VOPO_4$ nanosheets is always sustained on 0.96 V after initial irreversible reaction. In contrast, the overpotential of OH-$VOPO_4$ becomes much larger and the capacity gets much smaller just from 10th to 100th cycle (Figure S6, Supporting Information). Besides, the charge/discharge profiles of PA-$VOPO_4$ at 35 and 50 °C are shown in Figure S7 (Supporting Information), demonstrating the improvement of ion diffusion at elevated temperature. As compared in Figure 2d, the rate performance of PA-$VOPO_4$ nanosheets is quite remarkable among reported Mg-storage materials,[11,16,17,27–31] especially at relatively high current densities (>100 mA g^{-1}). The long-term cycling stability of the OH-$VOPO_4$ bulk and PA-$VOPO_4$ nanosheets is shown in Figure 2e. We can see that the capacity of OH-$VOPO_4$ drastically decreases,

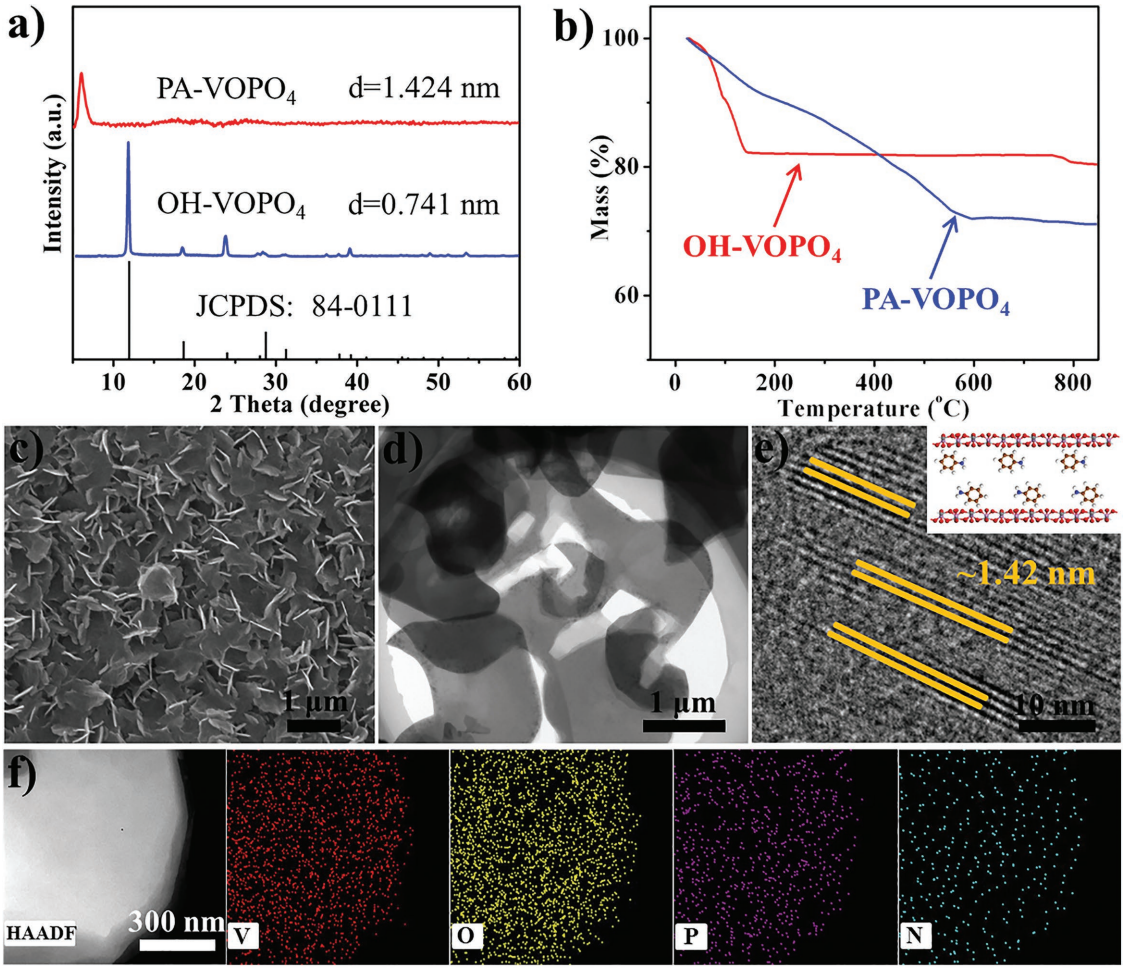

Figure 1. Structural and morphological characterization of the as-prepared $VOPO_4$. a) XRD patterns and b) TG analysis measured between room temperature and 800 °C with a heating rate of 5 °C min^{-1} under air atmosphere of OH-$VOPO_4$ bulk and PA-$VOPO_4$ nanosheets. c) SEM, d) TEM, and e) HRTEM images of PA-$VOPO_4$ nanosheets, and the inset is crystallographic model of PA intercalated $VOPO_4$-layered structure along the (001) plane. f) EDS color mapping images (V, O, P, and N elements) of PA-$VOPO_4$.

attributing to small interplanar distances for inflexible transmission. Besides, each interlayer of OH-$VOPO_4$ is coupled by weak hydrogen bonding,[19] in which H_2O molecules tend to skid off during repeated cation collision, probably resulting in the collapse of layered structure and the surface passivation of Mg anode. Nevertheless, the cycling stability of PA-$VOPO_4$ nanosheets achieves a great enhancement, which is capable of delivering 192 mAh g^{-1} of reversible capacity at 100 mA g^{-1} even after 500 cycles, related with the robust skeleton of PA-$VOPO_4$ nanosheets with expanded interlayer distance. The cycling property of PA-$VOPO_4$ nanosheets is equally out of the ordinary compared with other Mg-storage materials (Figure S8 and Table S1, Supporting Information). Figure S9 (Supporting Information) presents the electrochemical impedance spectroscopy (EIS) analysis performed on the fresh OH-$VOPO_4$ and PA-$VOPO_4$ electrode as well as cycled electrode at fully charged/discharged stage, suggesting that working cation of PA-$VOPO_4$ demonstrates low polarization and is not prone to trapped in the host,[27,32] beneficial for good rate capability and long cycle life.

Based on previous reports for lithium-/sodium-ion batteries (LIBs/SIBs), increasing the interlayer spacing facilitates lithium/sodium ion transport by creating a lower energy barrier,[22,23] which elaborates advantageous structural features for 2D ion transport channels and convenient ion diffusion pathways through controlling intercalating intercalants. PA-$VOPO_4$ with expanded layer spacing also exhibits better performance than those of OH-$VOPO_4$ for magnesium batteries, demonstrating that this effect can be extended from LIBs/SIBs to magnesium batteries.

Considering the complexity of intercalated species in APC electrolyte, we conducted chemical nature analysis of PA-$VOPO_4$ nanosheets at different charge/discharge states using XPS and EDS as well as mass change of electrodes. A hypothesis of $Mg^{2+}/MgCl^{+}$ insertion is given, and the plot of weight change of electrodes versus capacity is founded (**Figure 3**a,b). Then, the actual mass change of PA-$VOPO_4$ electrode is closed to operative mode of $MgCl^{+}$ insertion, while OH-$VOPO_4$ electrode corresponds to Mg^{2+} shuttling, preliminarily reflecting that the insertion species depends on interlayer spacing (Tables S2 and S3, Supporting Information). The increasing trend of the PA-$VOPO_4$ electrode mass is consistent with the theoretical mass change, revealing the PA molecules are immobile and

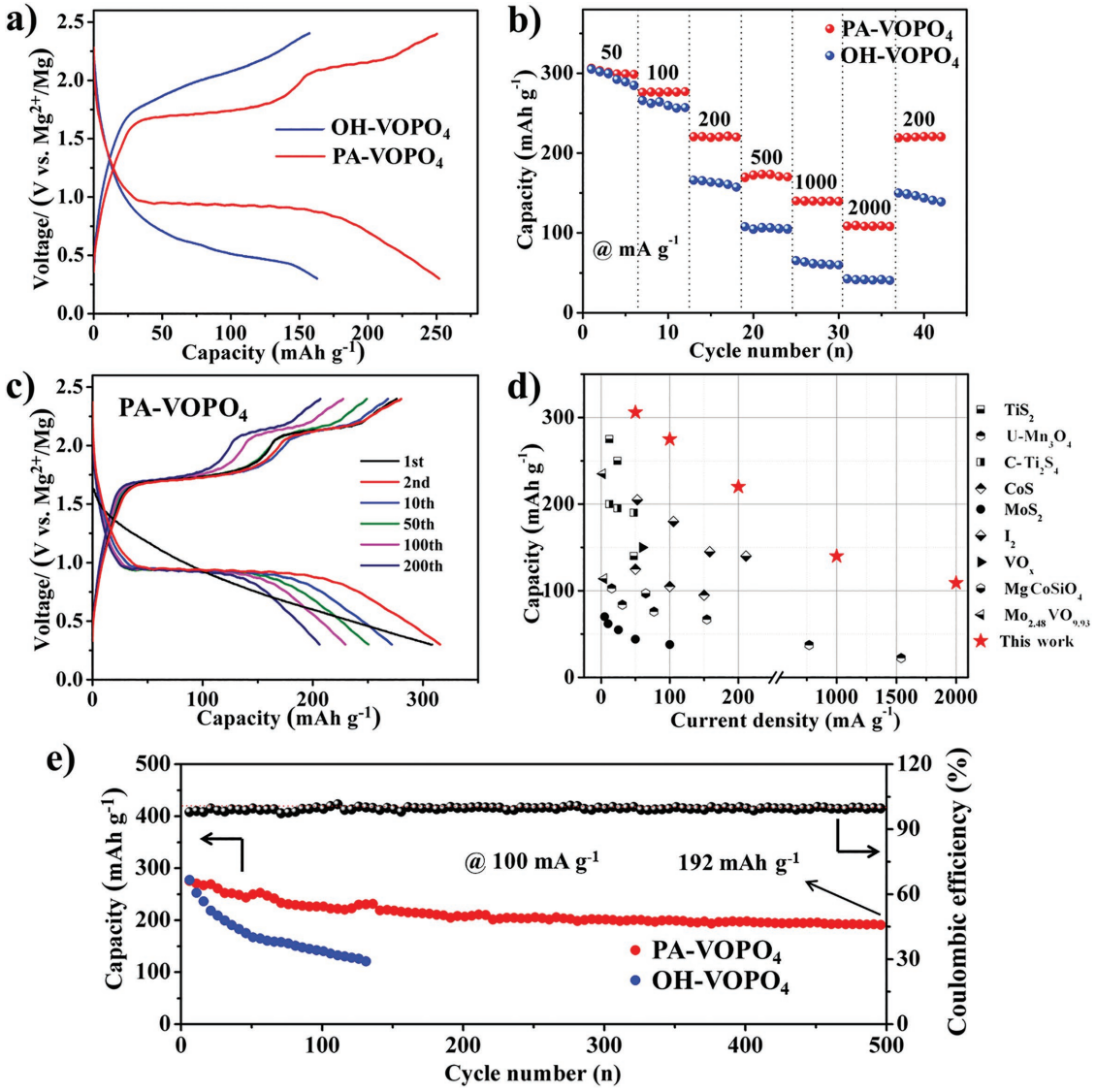

Figure 2. Mg-storage properties of $VOPO_4$. a) Charge/discharge profiles at 50th cycle, b) rate capability, and e) long-term cycling performance at 100 mA g^{-1} of the OH-$VOPO_4$ bulk and PA-$VOPO_4$ nanosheets. c) Charge/discharge curves of PA-$VOPO_4$ nanosheets at 100 mA g^{-1} at 1st, 2nd, 10th, 50th, 100th, 200th cycles. d) Comparison with other Mg-storage materials.

stay in the structure with no change. Compared with fresh electrode, the signals of Mg 1s and Cl 2p for PA-$VOPO_4$ simultaneously appear when discharging to 0.3 V, and the peak intensity concurrently decreases again on charging back to 2.4 V (Figure 3c,d), revealing Mg and Cl atoms together stepping into the structural interlayer. The cointercalation behavior was further evident by the analysis of EDS (Figure 3e), which determined the atomic ratio of inserted Mg to Cl to be 1 ± 0.2. The inductively coupled plasma (ICP) analysis also proves the ratio at fully discharged stage (Table S4, Supporting Information). The signal of N element at fully charged/discharged state indicates the existence of PA molecules in layered structure. The residual signals of Mg and Cl on fully charged electrode likely origin from irreversible reaction in the initial cycles (Figure 2c and Figure S10 (Supporting Information)) or the adsorbed species on the electrode surface. Integrated analysis of these results is that PA-$VOPO_4$ nanosheets with expanded interlayer spacing of 1.42 nm suffer from $MgCl^+$ shuttling. The intensity alternation of Mg and Cl peak for OH-$VOPO_4$ is shown in Figure S11 (Supporting Information), illustrating the OH-$VOPO_4$ with interlayer spacing of 0.74 nm allows Mg^{2+} to diffuse. Besides, the change of V elemental valence for PA-$VOPO_4$ during insertion/deinsertion process (Figure S12, Supporting Information) again confirms the robust configuration of PA-$VOPO_4$. The phase change of PA-$VOPO_4$ at charged/discharged state was also tracked through XRD measurement (Figure S13, Supporting Information). The peak of (001) plane slightly deviates to high angle on fully discharge, implying that the interlayer distance faces a bit shrink due to the interaction between $MgCl^+$ and host materials. As charge proceeds to 2.4 V, the reflex could recover to pristine position, illustrating that the expanded layered structure is well maintained. Figure 3f shows the structural

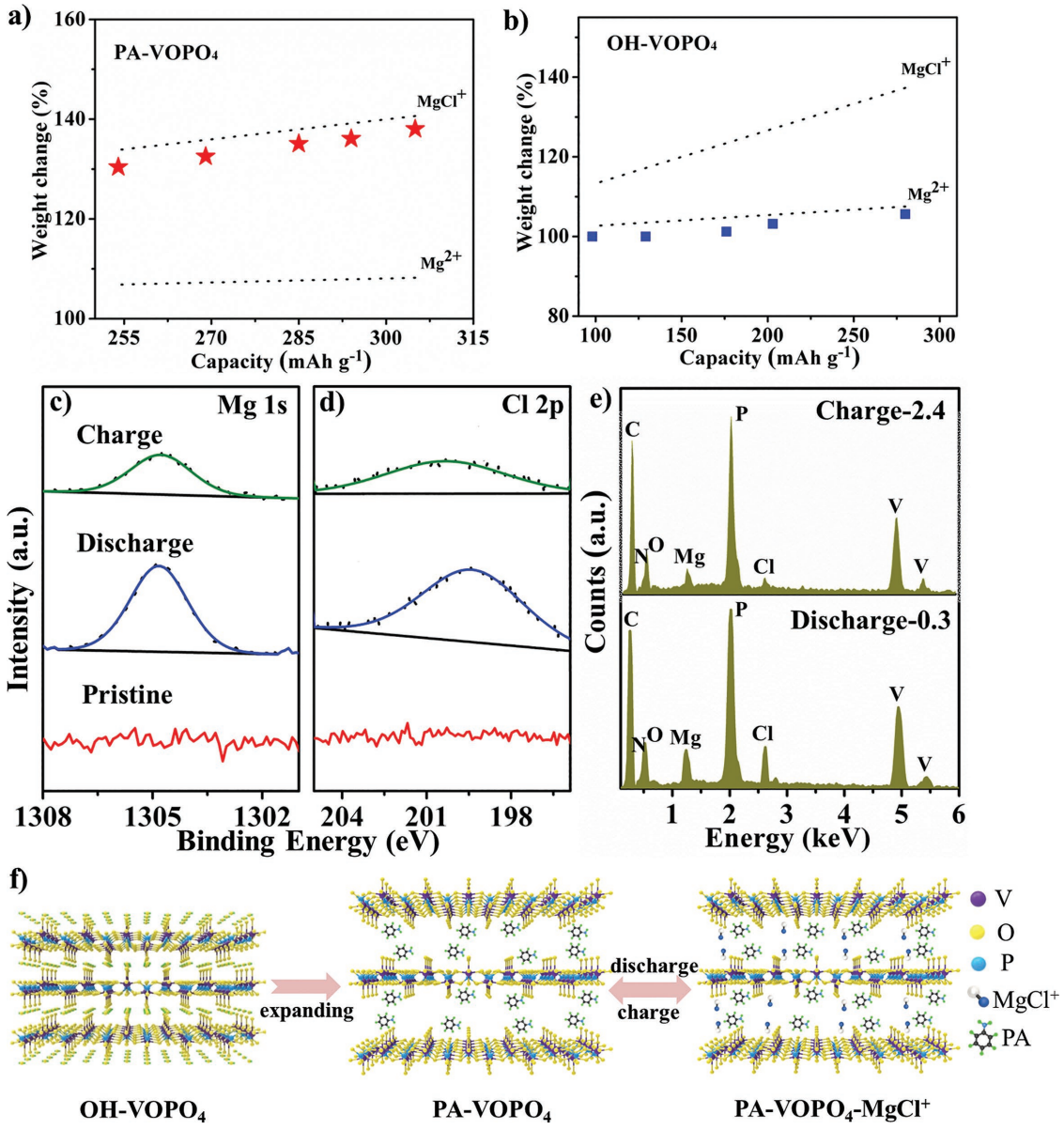

Figure 3. Chemical nature of intercalation species at different stages. Mass change of the electrodes upon discharge when a) PA-$VOPO_4$ nanosheets and b) OH-$VOPO_4$ bulk served as cathode materials. c,d) XPS spectra of Mg 1s (c) and Cl 2p (d), and e) EDS spectra for PA-$VOPO_4$ nanosheets at fully charged/discharged state. f) Schematic illustration of the experimental approach and proposed mechanism of PA-$VOPO_4$ nanosheets as Mg-storage materials.

optimization and Mg-inserted process of $VOPO_4$. The exchange of structural H_2O with PA molecule can effectively increase interlayer spacing of $VOPO_4$ from 0.74 to 1.42 nm, laying a good foundation for $MgCl^+$ as working cation to reduce polarization. The expanded interlayer spacing not only provides additional Mg-storage sites but also enhances the diffusion kinetics. As a result, PA-$VOPO_4$ delivers better rate performance and cycling life than those of OH-$VOPO_4$.

To probe into the discrepancy of Mg^{2+}/$MgCl^+$ dynamics, first-principle computations based on density functional theory (DFT) were performed to understand the diffusion behavior of two cations in PA-$VOPO_4$ nanosheets. In the light of previous work,[23] we considered two possible diffusion pathways (**Figure 4**a and Figure S14 (Supporting Information)) and calculated the energy profile and migration route by climbing-image nudged elastic band (CI-NEB) method implemented in VASP software.[33,34] Comparing the diffusion energy barriers of P1 and P2 pathways (Figure 4b), we conclude that both Mg^{2+} and $MgCl^+$ prefer the P1 pathway with lower migration energy in PA-$VOPO_4$ nanosheets. The $MgCl^+$ diffusion exhibits a lower energy barrier of 0.42 eV, whereas that of Mg^{2+} is 1.20 eV. According to Arrhenius formula ($D \propto \exp(-E_a/k_BT)$), the diffusion coefficient of $MgCl^+$ is 1.5×10^{13} times that of Mg^{2+}. The significant value suggests that designing material configuration for $MgCl^+$ migration is an immediate and favorable strategy to relieve diffusion kinetics issue of magnesium batteries,

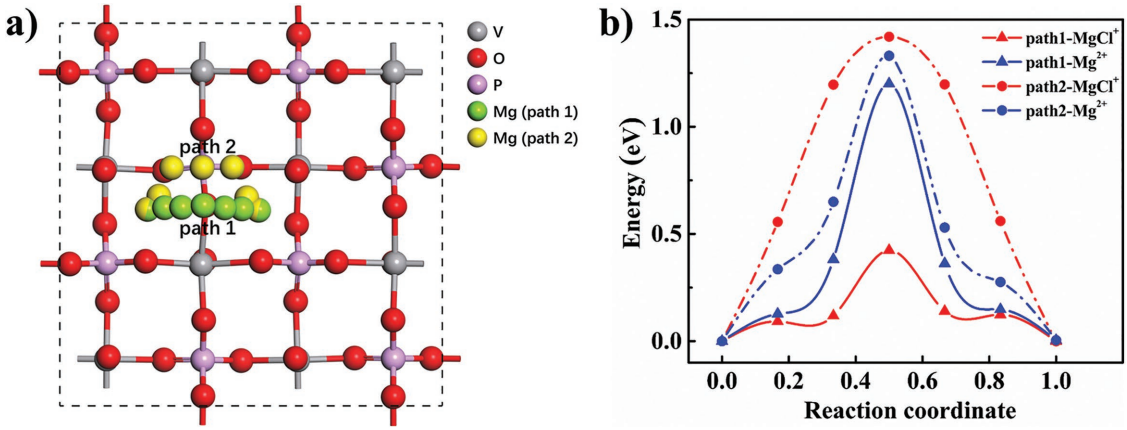

Figure 4. Diffusion barrier profiles of Mg^{2+}/$MgCl^{+}$ transport in PA-$VOPO_4$ nanosheets. a) Mg^{2+}/$MgCl^{+}$ diffusion routine. b) Diffusion energy barrier profiles of Mg^{2+}/$MgCl^{+}$ transport in PA-$VOPO_4$ nanosheets.

particularly in 2D-layered materials through interlayer-expanded approach. Combined computations with experimental evidence, PA-$VOPO_4$ nanosheets possess sufficient interlayer spacing for $MgCl^{+}$ to be taken in, conductive to decreasing polarization and further improving diffusion dynamics.

In summary, we have demonstrated the first application of $VOPO_4$ nanosheets with expanded interlayer spacing as novel robust cathode materials for rechargeable magnesium batteries. The expanded layer spacing established foundation to spur $MgCl^{+}$ insertion, which intrinsically reduces the polarity barrier and relieves diffusion kinetics issues together with the exposure of additional Mg-storage sites. Through first-principle computations, $MgCl^{+}$ intercalation affords the drastical drop of diffusion barrier and further diffusion coefficient increase of magnitudes compared with Mg^{2+}. As a result, the expanded $VOPO_4$ nanosheets exhibits a high reversible capacity of 310 mAh g^{-1} for magnesium batteries, high rate performance, and long cycle life (192 mAh g^{-1} even after 500 cycles at 100 mA g^{-1}). Combined with the merit of Mg anode, Mg/PA-$VOPO_4$ has a certain advantage compared with other battery system. This research may open a new avenue to develop rechargeable multivalence-ion batteries.

Supporting Information

Supporting Information is available from the Wiley Online Library or from the author.

Acknowledgements

This work was supported by the National Natural Science Fund for Distinguished Young Scholars (Grant No. 51425204), the National Natural Science Foundation of China (Grant Nos. 51521001, 51602239), the National Key Research and Development Program of China (Grant Nos. 2016YFA0202603, 2016YFA0202601), the Hubei Provincial Natural Science Foundation of China (Grant No. 2016CFB267), the International Science & Technology Cooperation Program of China (Grant No. 2013DFA50840), the Yellow Crane Talent (Science & Technology) Program of Wuhan City. K.Z. acknowledges the Korea Research Fellowship Program through the National Research Foundation of Korea (NRF) funded by the Ministry of Science, ICT and Future Planning (Grant No. 2016H1D3A1906790).

Conflict of Interest

The authors declare no conflict of interest.

Keywords

diffusion kinetics, interlayer spacing, magnesium batteries, $VOPO_4$ nanosheets

Received: March 28, 2018
Revised: May 17, 2018
Published online:

[1] B. Dunn, H. Kamath, J.-M. Tarascon, *Science* **2011**, *334*, 928.
[2] M. Armand, J.-M. Tarascon, *Nature* **2008**, *451*, 652.
[3] J. H. Miedema, H. C. Moll, *Resour. Policy* **2013**, *38*, 204.
[4] S. H. Mohr, G. M. Mudd, D. Giurco, *Minerals* **2012**, *2*, 65.
[5] P. Canepa, G. Sai Gautam, D. C. Hannah, R. Malik, M. Liu, K. G. Gallagher, K. A. Persson, G. Ceder, *Chem. Rev.* **2017**, *117*, 4287.
[6] H. D. Yoo, I. Shterenberg, Y. Gofer, G. Gershinsky, N. Pour, D. Aurbach, *Energy Environ. Sci.* **2013**, *6*, 2265.
[7] D. Aurbach, Z. Lu, A. Schechter, Y. Gofer, H. Gizbar, R. Turgeman, Y. Cohen, M. Moshkovich, E. Levi, *Nature* **2000**, *407*, 724.
[8] J. O. Besenhard, M. Winter, *ChemPhysChem* **2002**, *3*, 155.
[9] D. Aurbach, G. S. Suresh, E. Levi, A. Mitelman, O. Mizrahi, O. Chusid, M. Brunelli, *Adv. Mater.* **2007**, *19*, 4260.
[10] S. Su, Z. Huang, Y. NuLi, F. Tuerxun, J. Yang, J. Wang, *Chem. Commun.* **2015**, *51*, 2641.
[11] H. Tian, T. Gao, X. Li, X. Wang, C. Luo, X. Fan, C. Yang, L. Suo, Z. Ma, W. Han, C. Wang, *Nat. Commun.* **2017**, *8*, 14083.
[12] J. Xie, C. Li, Z. Cui, X. Guo, *Adv. Funct. Mater.* **2015**, *25*, 6519.
[13] Z. Zhang, B. Chen, H. Xu, Z. Cui, S. Dong, A. Du, J. Ma, Q. Wang, X. Zhou, G. Cui, *Adv. Funct. Mater.* **2018**, *28*, 1701718.
[14] H. D. Yoo, Y. Liang, H. Dong, J. Lin, H. Wang, Y. Liu, L. Ma, T. Wu, Y. Li, Q. Ru, Y. Jing, Q. An, W. Zhou, J. Guo, J. Lu, S. T. Pantelides, X. Qian, Y. Yao, *Nat. Commun.* **2017**, *8*, 339.
[15] Y. Liang, R. Feng, S. Yang, H. Ma, J. Liang, J. Chen, *Adv. Mater.* **2011**, *23*, 640.

[16] X. Sun, P. Bonnick, V. Duffort, M. Liu, Z. Rong, K. A. Persson, G. Ceder, L. F. Nazar, *Energy Environ. Sci.* **2016**, *9*, 2273.
[17] X. Sun, P. Bonnick, L. F. Nazar, *ACS Energy Lett.* **2016**, *1*, 297.
[18] K. Goubitz, P. Capkova, K. Melanova, W. Molleman, H. Schenk, *Acta Crystallogr.* **2001**, *B57*, 178.
[19] C. Wu, X. Lu, L. Peng, K. Xu, X. Peng, J. Huang, G. Yu, Y. Xie, *Nat. Commun.* **2013**, *4*, 2431.
[20] T. Nakato, Y. Furumi, N. Terao, T. Okuhara, *J. Mater. Chem.* **2000**, *10*, 737.
[21] A. De Stefanis, S. Foglia, A. A. G. Tomlinson, *J. Mater. Chem.* **1995**, *5*, 475.
[22] Y. Zhu, L. Peng, D. Chen, G. Yu, *Nano Lett.* **2017**, *16*, 742.
[23] L. Peng, Y. Zhu, X. Peng, Z. Fang, W. Chu, Y. Wang, Y. Xie, Y. Li, J. J. Cha, G. Yu, *Nano Lett.* **2017**, *17*, 6273.
[24] G. He, W. H. Kan, A. Manthiram, *Chem. Mater.* **2016**, *28*, 682.
[25] N. Kinomura, T. Toyama, N. Kumada, *Solid State Ionics* **1995**, *78*, 281.
[26] O. Mizrahi, N. Amir, E. Pollak, O. Chusid, V. Marks, H. Gottlieb, L. Larush, E. Zinigrad, D. Aurbach, *J. Electrochem. Soc.* **2008**, *155*, A103.
[27] L. Wang, K. Asheim, P. E. Vullum, A. M. Svensson, F. Vullum-Bruer, *Chem. Mater.* **2016**, *28*, 6459.
[28] W. Kaveevivitchai, A. J. Jacobson, *Chem. Mater.* **2016**, *28*, 4593.
[29] Y. Liang, H. D. Yoo, Y. Li, J. Shuai, H. A. Calderon, F. C. Robles Hernandez, L. C. Grabow, Y. Yao, *Nano Lett.* **2015**, *15*, 2194.
[30] D. He, D. Wu, J. Gao, X. Wu, X. Zeng, W. Ding, *J. Power Sources* **2015**, *294*, 643.
[31] Y. NuLi, Y. Zheng, Y. Wang, J. Yang, J. Wang, *J. Mater. Chem.* **2011**, *21*, 12437.
[32] P. Saha, P. H. Jampani, M. K. Datta, C. U. Okoli, A. Manivannan, P. N. Kumta, *J. Electrochem. Soc.* **2014**, *161*, A593.
[33] G. Henkelman, B. P. Uberuaga, H. Jónsson, *J. Chem. Phys.* **2000**, *113*, 9901.
[34] G. Kresse, *Phys. Rev. B* **1996**, *54*, 11169.